

# Phase preparation in steady-state free precession MR elastography<sup>☆</sup>

Jens Rump<sup>a</sup>, Carsten Warmuth<sup>a</sup>, Jürgen Braun<sup>b</sup>, Ingolf Sack<sup>a,\*</sup>

<sup>a</sup>Department of Radiology, Charité-Universitätsmedizin Berlin, Campus Charité Mitte, Charitéplatz 1, 10117 Berlin, Germany

<sup>b</sup>Institute of Medical Informatics, Charité-Universitätsmedizin Berlin, Campus Benjamin Franklin, Hindenburgdamm 30, 12200 Berlin, Germany

Received 21 February 2007; revised 29 May 2007; accepted 24 July 2007

## Abstract

Strain and motion measurements in balanced steady-state free precession (bSSFP) imaging require high magnetic field homogeneity. This requirement is due to the nonlinear signal response to spin phase variations in bSSFP. Here, a technique that utilizes background gradients for preparing strong in-plane spin phase variations is proposed. As a result, periodic patterns of increased motion sensitivity appear, which are interleaved with bands of low phase-to-noise ratio. Spatial filters commonly used in MR elastography (MRE) remove these bands and leave wave images equivalent to a uniform phase response in bSSFP-MRE. Since phase preparation gradients locally enhance motion sensitivity, the technique can be employed for selectively increasing the wave signal amplitude in MRE. The method is applied without the need for previous shimming, which reduces the examination time. In vivo phase prepared bSSFP-MRE is demonstrated in human liver and heart. © 2008 Elsevier Inc. All rights reserved.

**Keywords:** Magnetic resonance elastography; Balanced SSFP; Nonlinear phase response; Liver; Myocardium

## 1. Introduction

Palpation is the standard clinical practice for assessing the health of tissue near the body surface. The high sensitivity of the method to pathological changes is based on the direct relationship between the macroscopic viscoelastic properties of tissue and its structural organization on a molecular scale [1]. MR elastography (MRE) [2–4] allows quantifying the viscoelasticity of soft tissue deep inside the body and has the potential to help characterize, for instance, musculoskeletal diseases [5–7], liver fibrosis [8–10] or breast cancer [11–14].

Technically, MRE is based on the application of external vibrations and measuring the bulk tissue response by motion-sensitive MRI. The vibration frequency has to be low (for most in vivo studies, below 100 Hz) in order to mitigate damping of the shear waves due to viscosity. However, since in standard MRE, the duration of bipolar motion encoding gradients (MEGs) matches the mechanical vibration period,

low vibration frequencies automatically require long echo times and therefore impose high signal loss due to T2 dephasing. This concept was recently revised using MEGs much shorter than one vibration period [10,15,16]. In this approach, only fractions of one vibration cycle are exploited for motion encoding, resulting in lower motion sensitivity. Nevertheless, the concept of fractional MRE has two advantages: The experiment is accelerated, and shortening TE and TR allows the application of steady-state free precession (SSFP) sequences for encoding shear vibrations with high phase-to-noise ratio (PNR) in soft and viscous materials. This was shown to be beneficial in MRE studies on human liver and heart.

In SSFP-MRE, the harmonic vibration frequency has to be tuned to the sequence TR to avoid signal ghosts [17]. To combine short TR and low vibration frequencies  $f_v$ , one has to adjust both so that  $n \cdot TR = 1/f_v$ , with  $n$  being an integer number. In a recently published study, Bieri et al. [18] showed that altering the deflection amplitude of each TR results in two steady states of the magnetization, and thus, two images with inverse motion phase contrast (PC) have to be sampled in an interleaved fashion. In general,  $k$ -space must be sampled  $n$  times in fractional MRE. Fig. 1 depicts the motion encoding and sampling scheme for  $n=1, 2$  and 4

<sup>☆</sup> This study was supported by the German Research Foundation (Sa/901-2).

\* Corresponding author.

E-mail address: [ingolf.sack@charite.de](mailto:ingolf.sack@charite.de) (I. Sack).

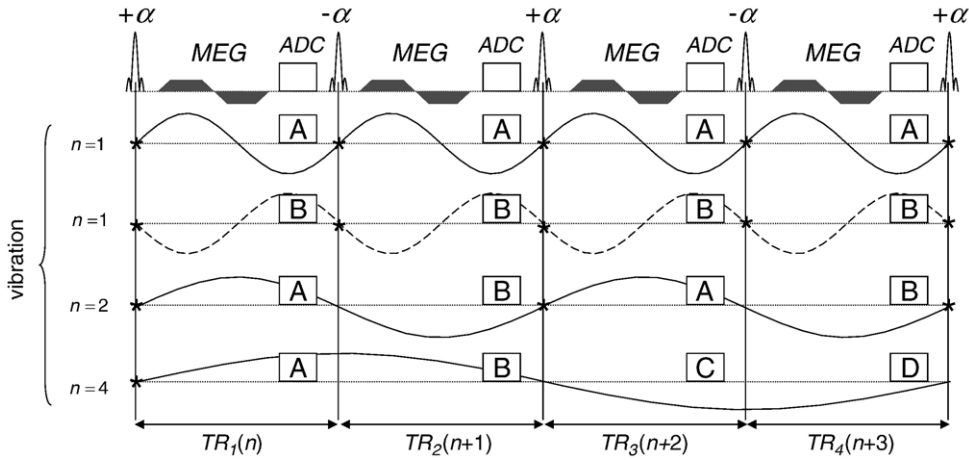


Fig. 1. Scheme of fractional motion encoding sequences in steady-state MRE. The progression of excitation pulses with alternating angle ( $+\alpha$ ,  $-\alpha$ ), MEGs and signal acquisition (ADC) is shown for three different matches of vibration frequency and TR ( $n=1$ , 2 and 4). Using  $n=1$ , a second experiment with reversed motion contrast has to be performed, either with a 180° shift in motion phase as displayed by the dashed line or with opposite MEG polarity (not shown). Asterisks demarcate the wave trigger.

used in the following experiments without being termed *fractional* in the further course.

It is well known that the relationship between phase increment per TR ( $\varphi_0$ ) and the resulting steady-state spin

phase  $\varphi$  in balanced SSFP (bSSFP) is nonlinear [19]. Inhomogeneous magnetic fields thus lead to an enhancement or attenuation of PC depending on the local off-resonance frequency. Bieri et al. [18] described a 10-fold PC

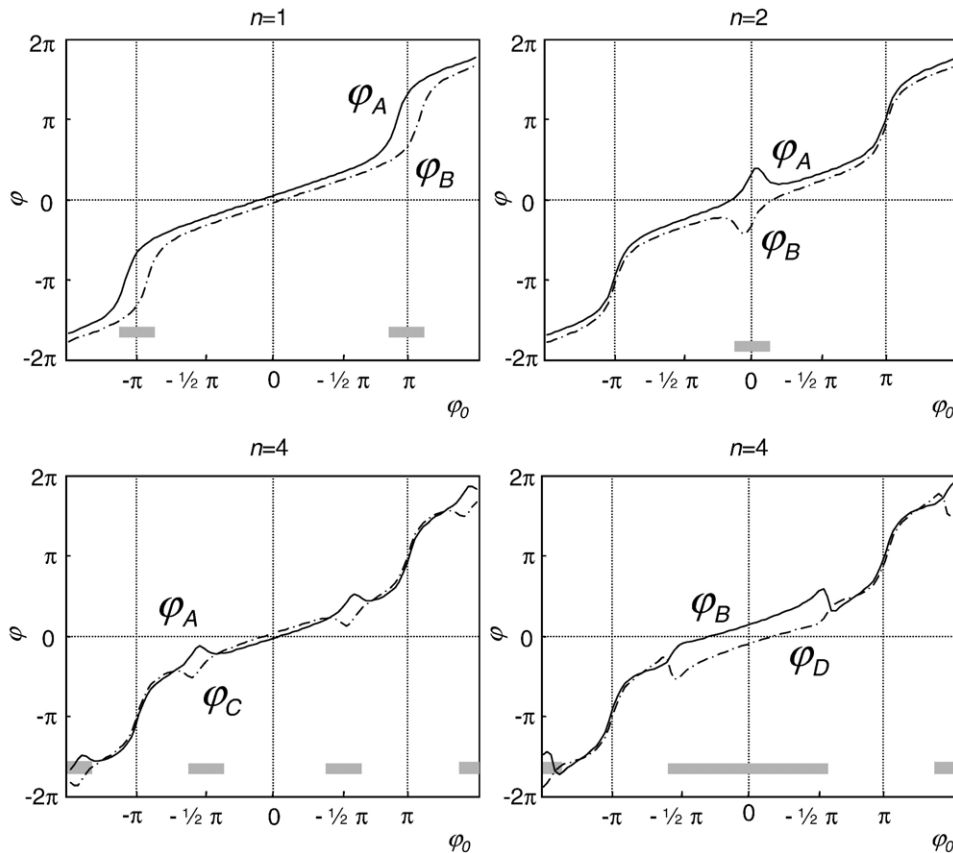


Fig. 2. Simulations of the nonlinear phase response in bSSFP-MRE with  $n=1$ , 2 and 4. The indices of  $\varphi$  correspond to the ADC labels of Fig. 1. Gray bars indicate the approximated range of  $\Delta\varphi$  enhancement. For  $n=4$ ,  $\varphi(\varphi_0)$  depends on the vibration phase relative to the MEG; thus, two graphs are plotted, which represent the 90° shift of the harmonic tissue deflection from A to B and from C to D according to Fig. 1. Simulations were performed using a maximum motion-induced phase shift of  $\pi/10$ .

enhancement in MRE experiments with bSSFP readout. However, this gain in PC is limited to a small frequency range around resonance, i.e., it requires perfect shimming, which is hard to achieve in vivo. Based on their work and the idea of fractional motion encoding, an experiment is introduced herein that adds background gradients to produce defined field inhomogeneities. As a result, periodic regions of enhanced and attenuated PNR appear in the phase difference images. This ensures that the averaged PC in the investigated object is independent of the  $B_0$  field distribution caused by susceptibility variations.

In the following, simulations of the nonlinear phase response in bSSFP-MRE are performed. Phantom experiments verify the effect of phase preparation gradients (PPGs), while experiments in human liver and heart show the in vivo applicability of the technique.

## 2. Simulations

Fig. 2 shows simulations of the phase response  $\varphi$  as a function of the phase increment per TR  $\varphi_0$ . Simulations of  $\Delta\varphi(\varphi_0)$  were performed using a numerical integration of Bloch's equations for a monochromatic spin at  $x, y, z=0$  in the gradient reference frame. The graphs are drawn for the accumulated phases  $\varphi_A, \varphi_B, \varphi_C$  and  $\varphi_D$  with subscripts corresponding to the ADC labels in Fig. 1. As it is standard in PC-MRI, two images of the inverse motion phase are subtracted from each other to produce a phase difference contrast  $\Delta\varphi$ . The sign of the motion phase is inverted in the course of one motion cycle after  $n \cdot \text{TR}/2$ . Hence, the wave image can be calculated as  $\Delta\varphi = \varphi_A - \varphi_B$  for  $n=1$  or  $n=2$  and as a complex phase image by  $\Delta\varphi = \varphi_A - \varphi_C + i(\varphi_B - \varphi_D)$  for  $n=4$ . Fig. 2 shows the dependency of  $\Delta\varphi$  on  $\varphi_0$ . In the range of linear phase response (e.g., between  $\pm\pi/2$  for  $n=1$ ), the

Table 1  
Sequence parameters

Parameter	Phantom	Liver	Heart
TR (ms)	6.31	8.13	5.31
$f_v$ (Hz)	158.5 ( $n=1$ ) 79.3 ( $n=2$ ) 40.0 ( $n=4$ )	61.8 ( $n=2$ )	47.5 ( $n=4$ )
MEG (in slice direction)	2 ms at 30 mT/m	5 ms at 35 mT/m	2 ms at 35 mT/m
PPG <sup>a</sup> (in read direction)	0.52 ms at 0.75 mT/m	0.52 ms at 0 mT/m 0.52 ms at 0.88 mT/m 0.52 ms at 1.28 mT/m 0.52 ms at 6.09 mT/m	0.52 ms at 0.52 mT/m 1.13 mT/m
FOV (mm <sup>2</sup> )	200×200	320×240	260×260
Matrix	128×128	128×96	128×64
Slice thickness (mm)	5	10	5
Flip angle ( $\alpha$ )	50°	20°	50°

FOV = field of view.

<sup>a</sup> Amplitudes corresponding to rectangular gradients.

motion sensitivity is approximately half that of standard nonbalanced PC-MRI. The highest sensitivity with  $n=1$  (i.e., largest difference between  $\varphi_A$  and  $\varphi_B$ ) is obtained at odd integer multiples of  $\varphi_0 = \pm\pi$ . Unfortunately, at these positions, the signal magnitude is strongly decreased and seen as dark banding in the images. With  $n=2$ , the highest  $\Delta\varphi$  is achieved at  $\varphi_0=0$  or multiples of  $\varphi_0 = \pm 2\pi$ , while  $n=4$  results in enhancement of  $\Delta\varphi$  at multiples of  $\varphi_0 = \pm\pi/2$ . In both of these cases, the areas of PC enhancement are not impaired by a loss of signal.

Obviously,  $\varphi_0=0$  throughout the entire region of interest (ROI) would be optimal for experiments with  $n=2$ , while  $\varphi_0 = \pi/2$  would be desirable for  $n=4$ . However, such homogeneous shimming is not feasible in vivo. Thus, we propose using a PPG that induces a strong periodicity to the in-plane phase variations and to focus in the data evaluation on regions of PC enhancement. To avoid intravoxel banding, the strength of the PPG must be smaller than  $2\pi/(\gamma \cdot \tau \cdot \Delta x)$ , with  $\gamma$  as the gyromagnetic ratio of protons,  $\tau$  the duration of the PPG and  $\Delta x$  the pixel spacing. If done properly, this ensures that the same amount of PC enhancement and attenuation occurs in every ROI so that the average PC remains constant.

## 3. Experiments

Experiments were run on a 1.5-T Siemens scanner (Siemens Magnetom Sonata, Erlangen, Germany). A bSSFP sequence was sensitized to motion using a single-cycle through-plane bipolar MEG between phase encoding and readout (Fig. 3). A PPG of 520  $\mu\text{s}$  duration was added after phase encoding in readout direction. A single-cycle sinusoidal current with duration  $1/f_v$  was fed each  $n$ th TR into an audio amplifier connected to a remote vibration generator as described in Ref. [10]. The maximum deflection

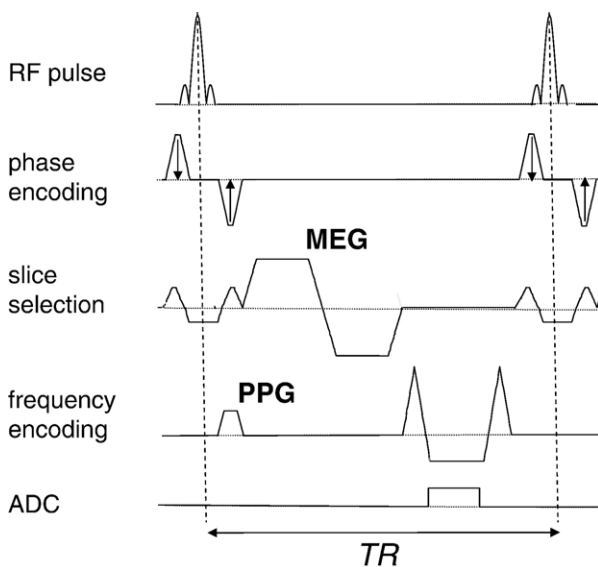


Fig. 3. Phase-prepared bSSFP-MRE sequence that is repeated in synchrony with the mechanical wave excitation as shown in Fig. 1.

amplitudes on the surface area of the volunteer were approximately 1 mm. The delay between the start of motion encoding and the trigger signal sent to the wave generator was shifted 16 times in a period of  $1/f_v$ , resulting in 16 phase difference wave images. Temporal Fourier transform was applied to the wave images, and the first harmonic vibration component was selected as complex wave image  $\Delta\varphi$  for further use.

### 3.1. Phantom studies

Phase-prepared bSSFP-MRE was tested on an agarose phantom (1.5%wt). Shear waves were introduced by a plate actuator attached to the top of the phantom. Acquisition parameters are listed in Table 1. The PPG used produced a phase shift of  $2\pi$  in 6 cm along the left–right direction. A profile of the phase difference in read direction representing  $\Delta\varphi(\varphi_0)$  was compared with the simulated phase difference.

### 3.2. In vivo studies on liver and heart

In vivo experiments were performed in a healthy 36-year-old male volunteer. For acquisition parameters, see Table 1. In liver studies, images were acquired with transversal orientation. The acquisition was completed in 24 s during

one breath-hold. The transducer was attached by Velcro strips onto the body surface over of the lower tip of the liver. Experiments were evaluated by complex modulus inversion based on Voigt’s model of a viscoelastic body after applying a spatial bandpass filter with isotropic band thresholds of  $k=10$  and 100/m to the complex wave data. Resulting elastograms were 2D median filtered (quadratic five-pixel neighborhood).

ECG-gated bSSFP-MRE experiments were applied to human myocardium. The image plane was aligned with the interventricular septum. The mechanical actuator was placed onto the thorax [20]. Images were acquired in 4 breath-holds of 32 heart cycles as described in Ref. [16]. The resulting 64 complex phase difference wave images  $\Delta\varphi=A-C+i(B-D)$  (Fig. 1) had a temporal resolution of nine vibration cycles (36 TR=191.2 ms).

## 4. Results

### 4.1. Phantom studies

Fig. 4 demonstrates the effect of a  $\varphi_0$  gradient in bSSFP-MRE for  $n=1, 2$  and 4. The first column ( $\Delta\varphi_a$ ) represents a widely homogeneous spin phase distribution

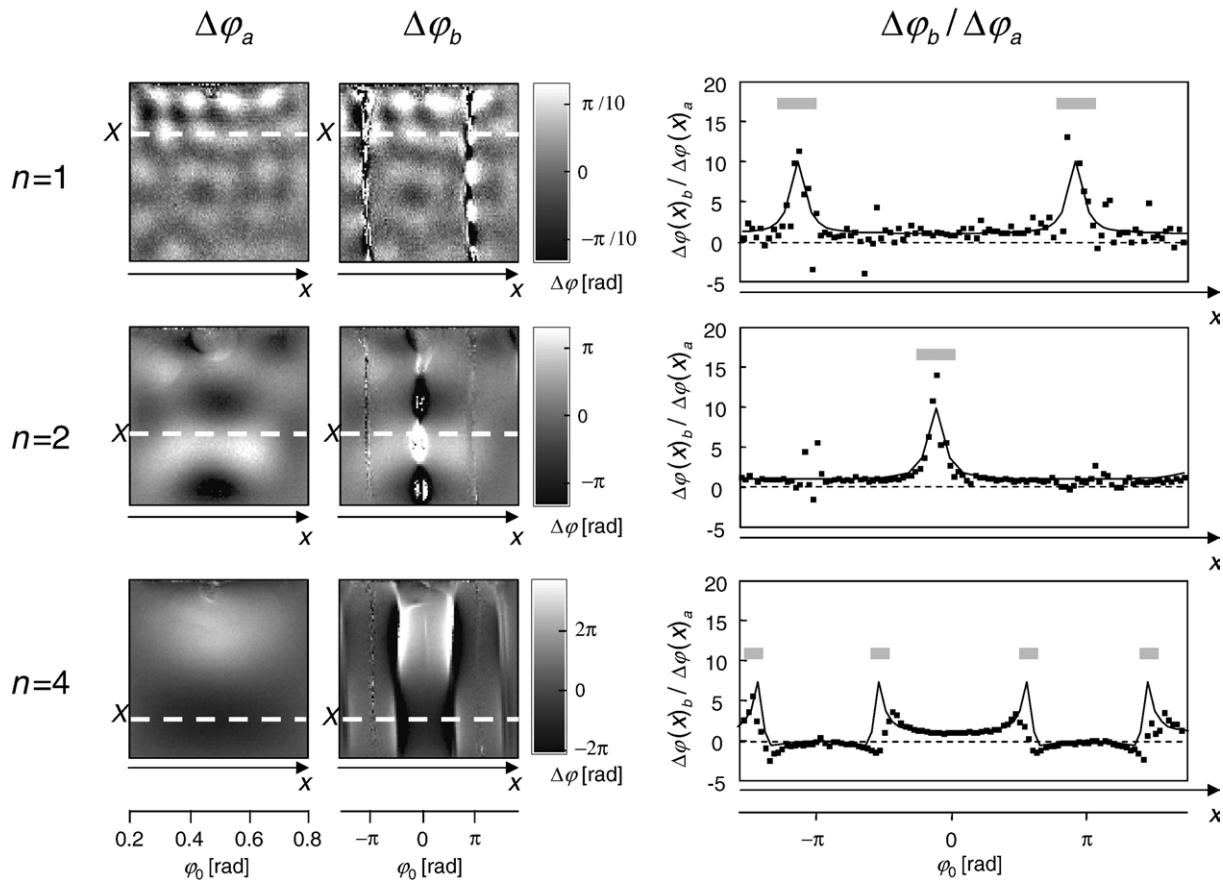


Fig. 4. Phase difference wave images in agarose without ( $\Delta\varphi_a$ ) and with ( $\Delta\varphi_b$ ) application of a weak PPG along the  $x$ -axis. The corresponding variation of  $\varphi_0$  is shown on the bottom. The third column ( $\Delta\varphi_b/\Delta\varphi_a$ ) shows the ratio of horizontal profiles through  $\Delta\varphi_a$  and  $\Delta\varphi_b$  (indicated there as dotted lines) superimposed to simulations. Gray bars correspond to demarcations of the phase enhancement as used in Fig. 2.

like that provided by the shimming system of our scanner. The variation of  $\varphi_0$  given on the bottom of each column was still between 0.2 and 0.8 rad (along the  $x$ -direction in the ROI). In this range, the response of  $\varphi$  to  $\varphi_0$  is linear for  $n=1, 2$  and 4 (cf. Fig. 2). Thus, the phase enhancement in these cases is uniform within the entire ROI. In contrast, the second column ( $\Delta\varphi_b$ ) demonstrates the effect of a nonuniform phase enhancement as a result of an additional PPG along the  $x$ -direction. The third column shows a comparison of measurement and simulation of the phase difference ratio  $\Delta\varphi_b/\Delta\varphi_a$  along the profiles X shown in the wave images. In the predicted regions demarcated by gray bars, an elevation of  $\Delta\varphi$  is seen with up to 10-fold amplification. The full width at half maximum indicates the motion-induced spin phase (the magnitude of the phase signal has to be considered for  $n=4$ ). The scattering of data

is increased around  $\varphi_0=\pm\pi$  corresponding to the low signal-to-noise ratio (SNR) in these regions.

#### 4.2. Liver studies

Fig. 5 shows measurements with increasing PPGs from 0 to 5.77 mT/m (Table 1). Magnitude images in the first row display the banding artifacts of decreasing width and distance resulting from the PPG. The initial banding pattern seen in A represents the effect of the intrinsic field inhomogeneities in the subject. With the TR used, first banding is seen at about 62 Hz off-resonance, which is far less than what can even be obtained with careful shimming in the abdomen. When applying a PPG, this pattern is overlaid with a periodic banding. In D, the intrinsic inhomogeneities are small compared to those induced by the PPG.

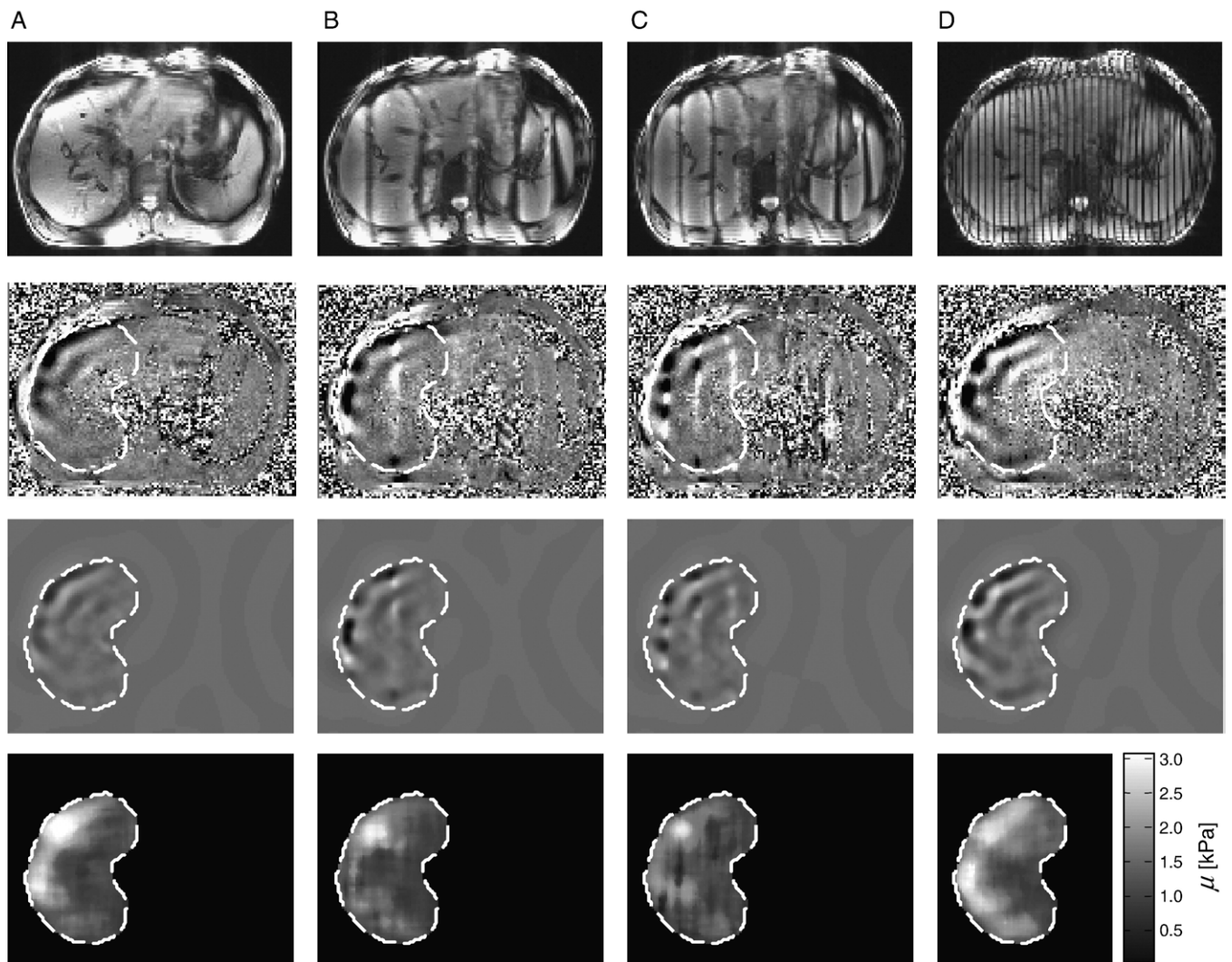


Fig. 5. Phase preparation in in vivo liver bSSFP-MRE ( $n=2$ ). First row, magnitude images; second row, raw phase difference  $\Delta\varphi$  with ROI (segmented liver, dashed line); third row,  $\Delta\varphi$  of the segmented liver after spatial filtering prior to wave inversion; fourth row, elastograms of the row above (real part representation after complex modulus inversion). The reference bSSFP-MRE experiment (without PPG) is shown in A. An increasing PPG in read direction (left–right) was applied from B (0.96 mT/m) to D (5.77 mT/m). For additional parameters, see Table 1.

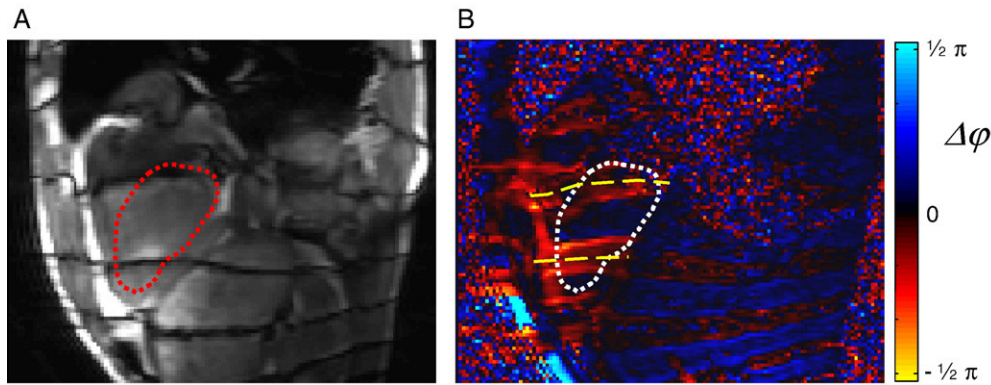


Fig. 6. In vivo myocardial bSSFP-MRE ( $n=4$ ). (A) Magnitude image. (B) Real part of the complex phase difference  $\Delta\varphi$ . The dotted line demarcates the interventricular septum. A PPG in vertical direction imposes  $\Delta\varphi$  enhancement along horizontal stripes at  $\varphi_0=\pm\pi/2$ . The positions of  $\varphi_0=\pm\pi$  in the septum (black bands in A) are indicated in B by yellow dashed lines.

The second row of Fig. 5 shows the respective phase difference wave images. The mean phase amplitudes in the ROI increase from A to D with 0.63, 0.88, 0.88 and 1.10 rad, which misindicates an increase of the mechanical deflection from A to D with 35, 46, 48 and 60  $\mu\text{m}$  if a linear phase response is assumed. In the nonlinear regime, the mean phase enhancement depends on the direction of wave normals relative to the orientation and positions of the PPG-induced bands of high motion sensitivity. This is seen in Fig. 5 (second row) where only in D the shear waves of high amplitude (i.e., in the vicinity of the upper right liver boundary) cross stripes of high motion sensitivity, and thus, the mean phase signal is highest there. The enhancement band width at half maximum of B reveals a motion-induced phase shift of  $1.14\pm 0.28$  rad corresponding to  $61\pm 15$   $\mu\text{m}$ . The third row of Fig. 5 demonstrates the removal of PPG banding by spatial bandpass filtering. These images were fed into a wave inversion program that yielded elastograms shown in the fourth row of Fig. 5. Mean shear moduli ( $\mu$ ) in the ROI were found with 2.0 (0.4), 1.7 (0.3), 1.6 (0.3) and 2.2 (0.2) kPa from A to D with S.D.'s given in brackets. The values were validated by a corresponding nonbalanced MRE experiment in the same volunteer, yielding  $2.5\pm 0.4$  kPa (data not shown). It is visible that the homogeneity of the elastogram is at its highest in D, while residues of PPG patterns still appear in B and C.

#### 4.3. Heart experiments

Fig. 6 demonstrates phase-prepared bSSFP-MRE in the human myocardium using  $n=4$ . The data shown were acquired in early systole. In A, the horizontal stripes of low SNR (at  $\varphi_0=\pm\pi$ ) are approximately 4 cm apart in the septum. Thus, the local enhancement of  $\Delta\varphi$  in B occurs at a distance of approximately 2 cm at  $\pm 1/2\pi$  as predicted by the simulations and phantom experiments shown in Fig. 4. The amount of phase enhancement in these regions was approximately four times that of a corresponding spoiled (nonbalanced) SSFP-MRE experiment with identical gradient timing, gradient amplitudes, TR and mechanical

vibration, as given in Table 1 (data not shown). This enhancement reaches 4/5 of the maximum achievable amount predicted by the simulations of Fig. 4C. There, a peak enhancement of 10 for  $n=4$  was found relative to the linear phase response in bSSFP, half of this value being relative to nonbalanced PC-MRI. The width of the peak enhancement at half maximum was below one pixel, indicating a wave deflection below 140  $\mu\text{m}$ . It is important to note that with  $n=4$ , the sign of  $\Delta\varphi$  alters near  $\varphi_0=\pm\pi/2$ , and thus, if the distance of the PPG bands had been reduced similar to the experiments shown in liver, a destructive interference of neighbored PPG bands degrades motion sensitivity. For this reason,  $n=4$  is not applicable when elastograms are desired.

## 5. Discussion

We have demonstrated the use of background gradients in bSSFP-MRE of human liver and heart. PPGs were used to produce periodic enhancement of motion sensitivity.

Homogeneity of motion sensitivity is a prerequisite for attributing variations of elastograms to viscoelastic tissue properties. Averaging the shear modulus over field inhomogeneities reduces the effect of variable  $\varphi_0$  on  $\mu$  as demonstrated in Fig. 5. There, the mean of  $\mu$  varies only slightly from A to D, while the distribution of elasticity appears different in all shown elastograms. In Fig. 5B and C, PPG-induced banding is still visible after wave inversion, while in D, the distance of the bands ( $\approx 7.5$  mm) is beyond the threshold of the spatial filter (10 mm) prior to the inversion. Thus, the application of spatial filters in MRE and the resulting reduction of spatial resolution enabled us to homogenize the bSSFP phase response. It is worthwhile to note that PPG banding can be removed by discarding higher spatial harmonics from  $k$ -space similar to the HARP analysis in tagged MRI [21].

A further increase of the PPG to 18 mT/m would reduce the distance of two bands down to voxel size

(2.5 mm). Then, the bSSFP signal theoretically shows no variations with field inhomogeneities. However, a slight misalignment of PPG pattern and image matrix results in a stroboscopic pattern sampling, i.e., the periodicity of the stripes depends on the degree of the misalignment. Additionally, such strong PPG acts as a dephaser gradient causing a loss in signal magnitude. This effect is mitigated by PPGs placed after the read gradient; however, the effect is still spoiling, which produces a mixture of bSSFP and flash imaging characteristics. In our experience, a band distance of two to four pixels corresponding to PPG amplitudes between 9 and 4.5 mT/m provides a well-balanced trade-off between field homogeneity and spatial resolution in bSSFP-MRE. Since shimming is not further needed, applying such standard background gradients considerably simplifies liver bSSFP-MRE and reduces the examination time.

The use of background gradients for a selected local enhancement of motion sensitivity was demonstrated in the human heart. Bipolar gradients with 2-ms durations to a mechanical vibration of approximately 50 Hz have a naturally low sensitivity. Thus, fractional motion encoding by  $n=4$  can significantly benefit from nonlinear phase response in bSSFP-MRE. Enhancement of the motion phase signal by a factor of 10 relative to the linear phase response in bSSFP-MRE and by a factor of 5 relative to nonbalanced MRE may be crucial for a successful application of MRE in the myocardium. Elastic properties of the heart may be deduced from relative changes of wave amplitudes during the cardiac cycle. The use of shear wave amplitudes observed by MRE for measuring elastic material properties was recently demonstrated in phantom experiments [22]. In this approach, the change of shear wave amplitudes is related to a change in the underlying elasticity. As such, the broadening of the enhancement bands near  $\varphi_0 = \pm 1/2\pi$  (Fig. 6) might provide a measure for detecting elasticity changes during the cardiac cycle. However, therefore, the spatial resolution of the phase enhancement bands has to be increased by decreasing the PPG strength to approximately 0.6 mT/m (yielding a 3.7-cm separation of the peak enhancement). Furthermore, the temporal resolution of  $\Delta\varphi$  need to be improved by reducing the number of lines in  $k$ -space sampled per heart cycle. The use of bSSFP-MRE for measuring myocardial elasticity is the subject of ongoing research. In this context, it is of fundamental importance to control local phase enhancement in the myocardium, as demonstrated in this study using  $n=4$ .

In summary, the nonlinear phase response in bSSFP-MRE yields local enhancement or local damping of encoded strain waves depending on the field inhomogeneities. This effect compromises the attribution of phase-signal variations to viscoelastic properties of the material. The proposed phase preparation technique converts field inhomogeneities to an in-plane field gradient, which is uniform in first approximation. The resulting aliasing of the nonlinear phase response produces a well-defined phase enhancement along

stripes perpendicular to the PPG direction, which can be used in bSSFP-MRE for calculating homogeneous elastograms or for the deduction of correct wave amplitudes. Beyond the scope of elastography, phase preparation can be utilized in bSSFP strain imaging to increase motion sensitivity or to treat field inhomogeneities without the need of extensive shimming.

## References

- [1] Fung Y. Biomechanics: mechanical properties of living tissue. New York: Springer-Verlag; 1993.
- [2] Muthupillai R, Lomas DJ, Rossman PJ, Greenleaf JF, Manduca A, Ehman RL. Magnetic resonance elastography by direct visualization of propagating acoustic strain waves. *Science* 1995;269(5232):1854–7.
- [3] Plewes DB, Betty I, Urchuk SN, Soutar I. Visualizing tissue compliance with MR imaging. *J Magn Reson Imaging* 1995;5(6):733–8.
- [4] Lewa CJ, De J, Certaines D. Viscoelastic property detection by elastic displacement NMR measurements. *J Magn Reson Imaging* 1996;6(4):652–6.
- [5] Basford JR, Jenkyn TR, An KN, Ehman RL, Heers G, Kaufman KR. Evaluation of healthy and diseased muscle with magnetic resonance elastography. *Arch Phys Med Rehabil* 2002;83(11):1530–6.
- [6] Ringleb SI, Bensamoun SF, Chen Q, Manduca A, An KN, Ehman RL. Applications of magnetic resonance elastography to healthy and pathologic skeletal muscle. *J Magn Reson Imaging* 2007;25(2):301–9.
- [7] Galban CJ, Maderwald S, Eggebrecht H, Grote W, de Greiff A, Uffmann K, et al. Monitoring the effects of chronic obstructive pulmonary disease on muscle elasticity by MR elastography. *Proceeding of the 13th Annual Meeting of ISMRM*; 2005. p. 2015. [Miami].
- [8] Huwart L, Peeters F, Sinkus R, Annet L, Salameh N, ter Beek LC, et al. Liver fibrosis: non-invasive assessment with MR elastography. *NMR Biomed* 2006;19(2):173–9.
- [9] Rouviere O, Yin M, Dresner MA, Rossman PJ, Burgart LJ, Fidler JL, et al. MR elastography of the liver: preliminary results. *Radiology* 2006;240(2):440–8.
- [10] Klatt D, Asbach P, Rump J, Papazoglou S, Somasundaram R, Modrow J, et al. In vivo determination of hepatic stiffness using steady-state free precession magnetic resonance elastography. *Invest Radiol* 2006;41(12):841–8.
- [11] Plewes DB, Bishop J, Samani A, Sciarretta J. Visualization and quantification of breast cancer biomechanical properties with magnetic resonance elastography. *Phys Med Biol* 2000;45(6):1591–610.
- [12] McKnight AL, Kugel JL, Rossman PJ, Manduca A, Hartmann LC, Ehman RL. MR elastography of breast cancer: preliminary results. *AJR Am J Roentgenol Am J Roentgenol* 2002;178(6):1411–7.
- [13] Van Houten EE, Doyley MM, Kennedy FE, Weaver JB, Paulsen KD. Initial in vivo experience with steady-state subzone-based MR elastography of the human breast. *J Magn Reson Imaging* 2003;17(1):72–85.
- [14] Sinkus R, Tanter M, Xydeas T, Catheline S, Bercoff J, Fink M. Viscoelastic shear properties of in vivo breast lesions measured by MR elastography. *Magn Reson Imaging* 2005;23(2):159–65.
- [15] Papazoglou S, Rump J, Braun J, Sack I. Shear-wave group-velocity inversion in MR elastography of human skeletal muscle. *Magn Reson Med* 2006;56(3):489–97.
- [16] Rump J, Klatt D, Braun J, Warmuth C, Sack I. Fractional encoding of harmonic motions in MR elastography. *Magn Reson Med* 2007;57(2):388–95.
- [17] Wood ML, Henkelman RM. MR image artifacts from periodic motion. *Med Phys* 1985;12(2):143–51.
- [18] Bieri O, Maderwald S, Ladd ME, Scheffler K. Balanced alternating steady-state elastography. *Magn Reson Med* 2006;55(2):233–41.

- [19] Haacke EM, Brown RW, Thompson MR, Venkatesan R. *Magnetic resonance imaging: physical principles and sequence design*. New York: John Wiley & Sons; 1999.
- [20] Rump J, Papazoglou S, Klatt D, Hamhaber U, Braun J, Sack I. In vivo MR elastography of the human heart: initial results. Proc 14th Annual Meeting ISMRM; 2006. p. 149 [Seattle].
- [21] Osman NF, Kerwin WS, McVeigh ER, Prince JL. Cardiac motion tracking using CINE harmonic phase (HARP) magnetic resonance imaging. *Magn Reson Med* 1999;42(6):1048–60.
- [22] Papazoglou S, Hamhaber U, Braun J, Sack I. Horizontal shear wave scattering from a nonwelded interface observed by magnetic resonance elastography. *Phys Med Biol* 2007;52(3):675–84.